

Curving THz Beams in the Near Field: A Framework To Compute Link Budgets

Hichem Guerboukha¹, Bin Zhao², Zhaoji Fang³, Edward Knightly², and Daniel M. Mittleman³

¹ Electrical and Computer Engineering, University of Missouri-Kansas City, Kansas City MO, USA

² Department of Electrical and Computer Engineering, Rice University, Houston TX, USA

³ School of Engineering, Brown University, Providence RI, USA

* *hichem.guerboukha@umkc.edu*

Abstract—We present a framework to engineer the trajectory of curved THz beams in the near-field region, with a focus on computing link budgets.

Index Terms—Terahertz, electromagnetics, propagation, near-field, wireless communications, link budget.

I. INTRODUCTION

Operating in the millimeter and THz band (0.1 – 1.0 THz) is a key aspect shared by many visions of future wireless systems. In this spectrum, plenty of bandwidth allows for the transmission of ultra-high data rates, often reaching several hundreds of Gbit/s [1]. However, as frequencies extend into the THz band, propagation losses become significantly consequential. For example, free-space path loss at 300 GHz reaches 80 dB over a distance of just 1 meter. To mitigate these losses, a common strategy involves the use of high-gain antennas, which are capable of producing highly directional beams [2]. In turn, this characteristic renders THz links susceptible to blockage, particularly when obstructions such as people and objects disrupt the line-of-sight path [3].

Recently, there has been a surge of interest in studying the near-field region for THz communications [4-12]. This region is especially relevant at THz frequencies since users in a THz wireless local area network (WLAN) could realistically be located in the near field of the base station. To illustrate this,

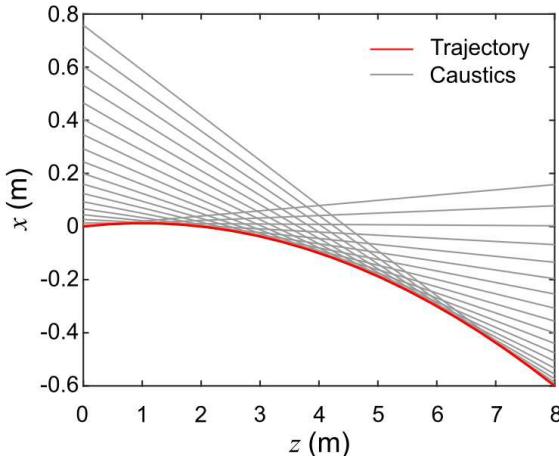


Fig.1 Trajectory engineering using caustics

consider that with a 10-cm aperture operating at 3 GHz, the

near-field region extends only up to 20 cm. However, the same 10-cm aperture size at 300 GHz results in a near-field extending to 20 m.

In this work, we show that the near-field physics can be exploited to realize exotic beams that have no equivalent in the far-field. We introduce the use of self-accelerating beams as an opportunity to solve challenges associated to blockage. These beams have the valuable characteristic of being able to follow arbitrary curved trajectories as they propagate within the near-field region of the transmitter. They have been studied at optical frequencies [13-14] in applications such as microscopy [15], particle manipulation [16], and laser machining [17]. This study focuses on their potential application in THz wireless communications. We establish a mathematical framework for engineering the trajectory of these beams and computing their near-field propagation. We also conduct a comparative analysis with standard Gaussian beams, showcasing the superior performance of curved beams in terms of link budgets.

II. RESULTS

A. Trajectory Engineering by Caustic Beam Design

Self-accelerating beams have the property of being able to propagate along curved trajectories in free space. More importantly, the trajectory of propagation can be engineered using the concept of caustics in ray optics [18]. Consider the geometry depicted in Fig. 1 where we wish to generate the trajectory defined by the red curve, in this case a parabola of expression $g(z) = -0.0125(z - 1)^2 + 0.0025$, with z in meters. To realize this trajectory, we define caustics along the trajectory. Shown as gray lines, these correspond to the set of lines that intersect the trajectory at the tangents. For a point $(z_i, g(z_i))$ of index i on the trajectory, the associated caustic is the line:

$$c_i(z) = \left. \frac{dg(z)}{dz} \right|_{z=z_i} z + g(z_i) - \left. \frac{dg(z)}{dz} \right|_{z=z_i} z_i \quad 1$$

By definition of the differential operator, these caustics make an angle θ with the x -axis: $\tan \theta = dg(z)/dz$. The phase profile at the input plane $\phi(x)$ can be found using the generalized Snell's law: $k_0 \sin \theta = d\phi(x)/dx$, with $k_0 = 2\pi/\lambda$ the free space wavenumber. Using trigonometry, we can relate the required phase profile to the desired trajectory:

$$\phi(x) = \frac{2\pi}{\lambda} \int \frac{dg(z)/dz}{\sqrt{1 + (dg(z)/dz)^2}} dx \quad 2$$

With this approach, any convex function (i.e., in which caustics only intersect the trajectory once at the tangent) can be realized. The geometric construction depicted in Fig. 1 also reveals limitations in the possible curvature of the trajectory originating from the aperture size. Considering two points on the trajectory: $(z_1, g(z_1))$ and $(z_2, g(z_2))$, the required aperture size D is directly related to the distance between the intersection of the caustics to the input plane:

$$D = \left| \left(g(z_2) - \frac{dg(z)}{dz} \Big|_{z=z_2} z_2 \right) - \left(g(z_1) - \frac{dg(z)}{dz} \Big|_{z=z_1} z_1 \right) \right| \quad 3$$

For example, to realize the trajectory depicted in Fig. 1 over the range of z from 0 m to 1 m, a 12.5 mm aperture would be required, while realizing the same trajectory up to 5 m would require a 312.5 mm aperture.

B. Failure of Friis Equation in the Near-Field

In typical far-field scenarios, the Friis equations is used to calculate link budgets. This equation – which relates the received power P_{Rx} to the transmitted power P_{Tx} – can be written as:

$$\frac{P_{Rx}}{P_{Tx}} = G_{Tx}(\theta, \phi) G_{Rx}(\theta, \phi) \left(\frac{\lambda}{4\pi r} \right)^2 \quad 4$$

where r is the distance between the transmitter and receiver. $G_{Tx}(\theta, \phi)$ and $G_{Rx}(\theta, \phi)$ are the gains of the transmitter and receiver respectively. In general, these gains are related to the directivities and expressed as a function of the spherical coordinates θ and ϕ , while neglecting the third spherical coordinate r . This is because in the far-field assumption – which underlies Friis equation, waves are considered spherical, and thus received powers decrease with the distance as $1/r^2$. Therefore, the third spherical coordinate is integrated in the free-space path loss term: $(\lambda/4\pi r)^2$.

This aspect is important in distinguishing the regimes of near-field and far-field propagation. In the near-field, waves are not necessarily spherical, and powers do not necessarily fall as $1/r^2$. Consider for example the case of a focused beam. There, it is clear that, as the receiver moves in the optical axis, the power increases until the receiver reaches the focal plane, then starts to decrease as the receiver distance itself from the focus. This non-monotonous behavior is a clear indication that powers do not follow the $1/r^2$ law. Moreover, range-independent values of the gains (as typically defined in the far-field) have no direct equivalent in the near-field. One must therefore carefully calculate link budget in the near field, which we do in the following.

C. Huygens-Fresnel Principle

To compute near-field link budgets, we resort to calculating the fields using the Huygens-Fresnel principle, which states that the field at the output plane is the summation of infinitesimal spherical sources emanating from the input

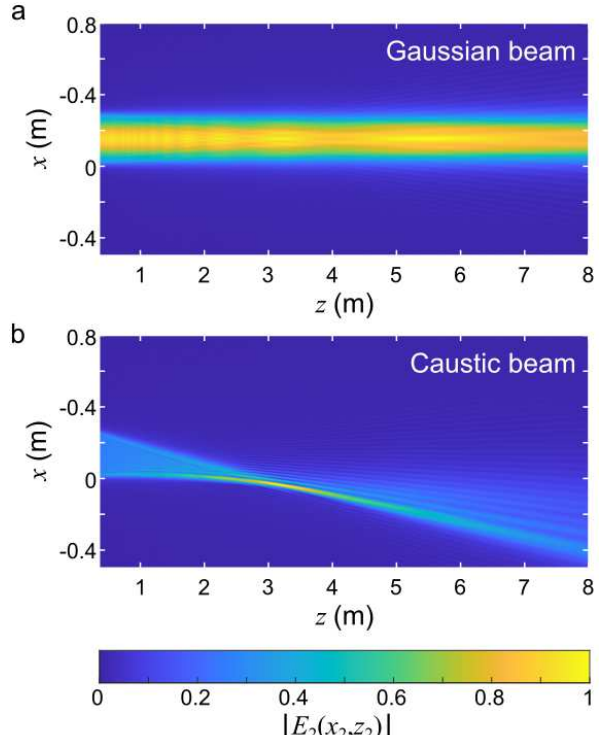


Fig.2 Near-field propagation of (a) a Gaussian beam and (b) a caustic beam.

plane [19]. Mathematically, this leads to a diffraction integral, which we derive in the following.

Consider an input aperture located at the $z = 0$ plane, with a coordinate $(x_1, y_1, 0)$, and an observation plane located at $z = z_2$, with a coordinate (x_2, y_2, z_2) . Assume a complex field profile $E_1(x, y)$ at the aperture plane, consisting of both an amplitude and phase profile. The field on the observation plane can be computed using the diffraction integral:

$$E_2(x_2, y_2, z_2) = \frac{1}{j\lambda z_2} \iint_{S_1} E_1(x_1, y_1) \frac{\exp(jk|\vec{r}_{12}|)}{|\vec{r}_{12}|^2} dx_1 dy_1 \quad 4$$

with $|\vec{r}_{12}| = \sqrt{(x_2 - x_1)^2 + (y_2 - y_1)^2 + z_2^2}$ the distance between the observation point and the input point. We note that Eq. 4 is valid under the scalar approximation, which means that there is no coupling between the vector components of the electromagnetic field and that each of these components individually respects Eq. 4. This approximation is particularly valid in a linear, isotropic, homogeneous, and non-dispersive medium such as air, which is, for all practical intent, where we want to calculate link budgets. To avoid coupling between the vector components of the field, we assume that the input plane is located wavelengths away from the antenna, to avoid any reactive near-field effect such as surface waves, back-coupling, etc. In practice, one could run a numerical simulation to compute the response of the transmitter antenna in the reactive near-field region, and then use Eq. 4 to calculate its response in the radiative near-field.

D. Approximation for Separable Input Aperture Function

We note that Eq. 4 demands considerable computing power, particularly for large input aperture sizes as required for near-field operation. The Fresnel approximation is commonly used to simplify the integral. Under this approximation, the distance term $|\vec{r}_{12}|$ is approximated differently whether it appears in the denominator or the exponential in Eq. 4. Using the binomial expansion, in the denominator it becomes $|\vec{r}_{12}| \approx z$, while in the exponential it is $|\vec{r}_{12}| \approx z \left[1 + \frac{1}{2} \left(\frac{x_2 - x_1}{z} \right)^2 + \frac{1}{2} \left(\frac{y_2 - y_1}{z} \right)^2 \right]$.

Furthermore, we consider that the input aperture is a separable function of the form:

$$E_1(x_1, y_1) = E_1^x(x_1) E_1^y(y_1) \quad 5$$

With these approximations, Eq. 4 can be separated in two unidimensional integrals:

$$E_2(x_2, y_2) = S_x(x_2, z_2) S_y(y_2, z_2) \quad 6$$

where

$$S_x = \frac{e^{\frac{jk}{2}(z_2 + \frac{x_2^2}{z})}}{\sqrt{j\lambda z}} \int E_1^x(x_1) \exp \left[\frac{jk}{z_2} \left(\frac{x_1^2}{2} - x_2 x_1 \right) \right] dx_1 \quad 7$$

and

$$S_y = \frac{e^{\frac{jk}{2}(z_2 + \frac{y_2^2}{z})}}{\sqrt{j\lambda z}} \int E_1^y(y_1) \exp \left[\frac{jk}{z_2} \left(\frac{y_1^2}{2} - y_2 y_1 \right) \right] dy_1 \quad 8$$

Using Eq. 6 with the unidimensional integrals brings an important reduction in the number of points to calculate. As a comparison, calculating Eq. 4 for an input aperture of 30 cm operating at 300 GHz and an output aperture of 1 cm would require summation of 144 million points (considering a $\lambda/2$ discretization over the aperture). The same input and output apertures would require 12,000 points using the approach of Eq. 6; this is a considerable and non-negligible improvement.

E. Near-Field Propagation

We now present results of the near-field propagation of a caustic beam, and we compare these to those of a Gaussian beam. We consider a square input aperture of $30 \times 10 \text{ cm}^2$, and a frequency of operation of 200 GHz. The caustics beam is designed to realize the parabolic trajectory $g(z) = -0.0125(z - 1)^2 + 0.0025$, with z in meters. Using Eq. 2, we calculate the phase profile $\phi(x)$, which serves as the phase term in the complex field:

$$E_1^x(x_1) = \exp(j\phi(x)) \quad (\text{caustics}) \quad 9$$

For comparison purposes, we also consider a Gaussian beam with a flat zero input phase:

$$E_1^x(x_1) = \exp(-2 \ln 2 x^2 / \text{fwhm}^2) \quad (\text{Gaussian}) \quad 10$$

where we consider the full width at half maximum to be $\text{fwhm} = 15 \text{ cm}$. For both the caustic beam and the Gaussian, we assume a Gaussian with a fwhm of 5 cm in the y direction.

Fig. 2 shows the computed field in the near-field region obtained using the procedure described in Eq. 6. The Gaussian

beam has a somewhat monotonic decrease of the field as a function of the distance, although we observe oscillations of the field close to the input aperture. These oscillations are a characteristic of near field propagation and can also be observed experimentally at optical wavelengths [20].

In comparison, as intended, the caustic beam bends in the near-field region following the designed trajectory. While curving, the field also peaks in amplitude (at approximately 3 m), in a behavior similar to focusing.

F. Received Power

To calculate the link budget, we also need to take into account characteristics of the receiver. From Fig. 2, it is worth noting that not only the location of the receiver in the xz plane matters, but also its size and angular positioning. Indeed, the power that traverses an aperture S_{Rx} can be calculated from the integral over the intensity:

$$P_{Rx} = \frac{1}{2Z_0} \iint_{S_{Rx}} |E_2(x, y, z_2)|^2 dS_{Rx} \quad 11$$

where Z_0 is the free-space impedance. In general, the received power depends on details about the receiver, specifically its radiated field (when operated as a transmitter by the antenna reciprocity principle). One can for example use a numerical simulation to obtain these fields in the reactive near field. Then, the amount of power that can effectively couple into the receiver can be calculated using power coupling integrals to yield the efficiency term, a number between 0 and 1 that indicate respectively no coupling and total coupling of the power.

In the following, however, for the discussion to remain agnostic with respect to the type of receiver, we assume perfect coupling of the field to the antenna. This means that we assume that the receiver can realize any phase and amplitude profile to match the incoming field without any

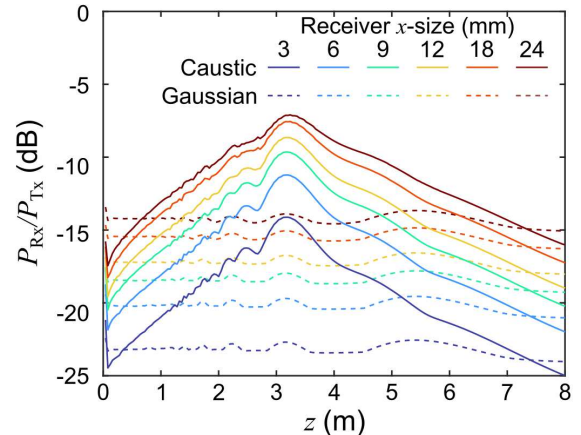


Fig. 2 Near-field link budget for a caustic and a Gaussian beam for different receiver sizes.

impedance mismatch. We also assume that the receiver has its aperture positioned parallel to the input plane. In other words, the following results have to be interpreted as the maximum power that could be detected.

Fig. 3 presents the link budget (the ratio of received to transmitted power) as a function of the distance z . In these calculations, we assume the aperture to be centered in x to the maximum of the radiated field. We perform the calculation for various aperture sizes in x (assuming a constant size of 10 mm in y). As can be seen, the caustic has a focused beam behavior, in which the link budget increases to reach its maximum at 3 m. In comparison, the Gaussian beam has a quasi-constant link budget over the considered range of 8 meters. In both cases, the link budget increases with the receiver size, which is simply a consequence that more energy can be captured by the antenna. Overall, for a same receiver size, the caustic beam outperforms the Gaussian beam across the range of ~ 0.5 m to 7.5m. This indicates that using caustic beam, beyond the curvature advantage, has also the advantage of capturing more power because of the focusing effect.

We mention that both beams were generated from an input aperture of 300 mm at 200 GHz. This allows the calculation to remain in the near-field region for both cases and allows for a fair comparison. However, it is interesting to also compare the case with a standard far-field scenario. At 3 meters (max caustic peak), free-space path loss at 200 GHz amounts to 88 dB. This means that to be able to realize the same performance of $P_{Rx}/P_{Tx} = -10$ dB as in the case of the caustic beam with a 12 mm receiver, 78 dB must be obtained by combining high gain antennas and high power. A typical horn antenna at 200 GHz provides 21 dB of gain [21]. Using a pair of those would still require 36 dB of additional transmitter power to reach the same figure of $P_{Rx}/P_{Tx} = -10$ dB. This highlights another important advantage of near-field links, in that they require considerably less power as their far-field counterpart. This is an important feature since power restrictions are one of the main concerns of future wireless networks.

III. CONCLUSION

In conclusion, we have presented a mathematical framework to engineer curved beams and compute link budgets in the near field. Curved beams can be engineered using the concept of caustics in ray optics, to realize arbitrary convex trajectories. Unlike far-field situations where link budgets can be calculated with Friis equation, link budgets in the near-field are calculated using a diffraction formulation of the Huygens-Fresnel principle. As an illustrative result, we calculated the near-field response of a caustics beam with a parabolic trajectory and compared it to that of a Gaussian beam. Our results show that caustics beam outperform Gaussian beams in terms of link budget. Our framework can further be improved by considering details about the receiver. These results can help future THz system designers to engineer curved beams that can curve around obstacles to mitigate blockage disruptions.

REFERENCES

- [1] S. Jia et al., "2 × 300 gbit/s line rate ps-64qam-OFDM thz photonic-wireless transmission," *Journal of Lightwave Technology*, vol. 38, no. 17, pp. 4715–4721, 2020.
- [2] P. Sen, J. V. Siles, N. Thawdar, and J. M. Jornet, "Multi-kilometre and multi-gigabit-per-second sub-terahertz communications for wireless backhaul applications," *Nature Electronics*, vol. 6, no. 2, pp. 164–175, 2022.
- [3] V. Petrov, M. Komarov, D. Molchanov, J. M. Jornet, and Y. Koucheryavy, "Interference and SINR in millimeter wave and terahertz communication systems with blocking and directional antennas," *IEEE Transactions on Wireless Communications*, vol. 16, no. 3, pp. 1791–1808, 2017.
- [4] V. Petrov, D. Bodet, and A. Singh, "Mobile near-field terahertz communications for 6G and 7G Networks: Research challenges," *Frontiers in Communications and Networks*, vol. 4, 2023.
- [5] A. Singh et al., "Wavefront Engineering: Realizing Efficient Terahertz Band Communications in 6G and Beyond," arXiv: 2305.12636 (2023).
- [6] M. Cui, Z. Wu, Y. Lu, X. Wei, and L. Dai, "Near-field mimo communications for 6G: Fundamentals, challenges, potentials, and future directions," *IEEE Communications Magazine*, vol. 61, no. 1, pp. 40–46, 2023.
- [7] A. Singh, V. Petrov, and J. M. Jornet, "Utilization of bessel beams in wideband sub terahertz communication systems to mitigate beamsplit effects in the near-field," *ICASSP 2023 - 2023 IEEE International Conference on Acoustics, Speech and Signal Processing (ICASSP)*, 2023.
- [8] I. V. A. K. Reddy et al., "Ultrabroadband terahertz-band communications with self-healing bessel beams," *Communications Engineering*, vol. 2, no. 1, 2023.
- [9] C. Han, Y. Chen, L. Yan, Z. Chen, and L. Dai, "Cross Far- and Near-field Wireless Communications in Terahertz Ultra-large Antenna Array Systems," arXiv:2301.03035 (2023).
- [10] K. Rouhi, S. E. Hosseininejad, S. Abadal, M. Khalily, and R. Tafazolli, "Multi-channel near-field terahertz communications using reprogrammable graphene-based digital metasurface," *Journal of Lightwave Technology*, vol. 39, no. 21, pp. 6893–6907, 2021.
- [11] W. Tang et al., "Wireless Communications with reconfigurable intelligent surface: Path loss modeling and experimental measurement," *IEEE Transactions on Wireless Communications*, vol. 20, no. 1, pp. 421–439, 2021.
- [12] W. Hao et al., "The far-/near-field beam squint and solutions for thz intelligent reflecting surface communications," *IEEE Transactions on Vehicular Technology*, vol. 72, no. 8, pp. 10107–10118, 2023.
- [13] N. K. Efremidis, Z. Chen, M. Segev, and D. N. Christodoulides, "Airy beams and accelerating waves: An overview of recent advances," *Optica*, vol. 6, no. 5, p. 686, 2019.
- [14] T. Ellenbogen, N. Voloch-Bloch, A. Ganany-Padowicz, and A. Arie, "Nonlinear generation and manipulation of airy beams," *Nature Photonics*, vol. 3, no. 7, pp. 395–398, 2009.
- [15] S. Jia, J. C. Vaughan, and X. Zhuang, "Isotropic three-dimensional super-resolution imaging with a self-bending point spread function," *Nature Photonics*, vol. 8, no. 4, pp. 302–306, 2014.
- [16] J. Baumgartl, M. Mazilu, and K. Dholakia, "Optically mediated particle clearing using airy wavepackets," *Nature Photonics*, vol. 2, no. 11, pp. 675–678, 2008.
- [17] A. Mathis et al., "Micromachining along a curve: Femtosecond laser micromachining of curved profiles in diamond and silicon using accelerating beams," *Applied Physics Letters*, vol. 101, no. 7, p. 071110, 2012.
- [18] L. Froehly et al., "Arbitrary accelerating micron-scale caustic beams in two and three dimensions," *Optics Express*, vol. 19, no. 17, p. 16455, 2011.
- [19] J. W. Goodman, *Introduction to Fourier Optics*. New York: McGraw-Hill, 2017
- [20] G. D. Gillen and S. Guha, "Modeling and propagation of near-field diffraction patterns: A more complete approach," *American Journal of Physics*, vol. 72, no. 9, pp. 1195–1201, 2004.

- [21] J. Ma, R. Shrestha, L. Moeller, and D. M. Mittleman, "Invited article: Channel Performance for indoor and outdoor terahertz wireless links," *APL Photonics*, vol. 3, no. 5, 2018. doi:10.1063/1.5014037